

Electronic Supplementary Information

Hollow structured medium entropy transition metal selenide CoNiFe-Se@NC enables high performance of sodium-ion batteries

Weijie Si¹, Siyuan Lai¹, Wendan Jiang¹, Kanghua Miao¹, Chao Wang^{2*}, Hongyu Wang^{3*}, Xiongwu Kang^{1*}

1 School of Environment and Energy, South China University of Technology, 382 East Waihuan Road, Higher Education Mega Center, Guangzhou, 510006, China

2 China Southern Power Grid Technology Co., Ltd., Guangzhou, 510080, China

3 School of Mechanical Engineering, Qinghai University, Xining, 810016, China.

E-mail: wangchaomly@163.com (C. Wang); HYuWang26@163.com (H. Wang);
esxkang@scut.edu.cn (X. Kang)

1. Experimental Section/Methods

1.1 Materials:

Cobalt nitrate hexahydrate ($\text{Co}(\text{NO}_3)_2 \cdot 6\text{H}_2\text{O}$), 2-methylimidazole (2-MeIM), nickel nitrate hexahydrate ($\text{Ni}(\text{NO}_3)_2 \cdot 6\text{H}_2\text{O}$), ferrous chloride tetrahydrate ($\text{FeCl}_2 \cdot 4\text{H}_2\text{O}$), dopamine hydrochloride (DAH), tris(hydroxymethyl)aminomethane (Tris) and selenium powder (Se) were all purchased from Energy Chemical Co., Ltd. Methanol and ethanol were purchased from Damao Chemical Reagent Factory. Separator (Whatman GF/D) and CR-2032 coin cell were bought from Canrd Technology Co. Ltd.

1.2 Synthesis of ZIF-67:

In a typical synthesis procedure, 0.04 mol of $\text{Co}(\text{NO}_3)_2 \cdot 6\text{H}_2\text{O}$ was dissolved in 500 mL methanol, designated as solution A. Simultaneously, 0.16 mol of 2-methylimidazole was dissolved in 500 mL methanol, designated as solution B. Solution A was gradually added to solution B, and the mixture was stirred for 24 hours. The resulting solution was centrifuged and the precipitate was washed three times with methanol. Finally, the precipitate was dried at 60 °C for 12 hours to obtain ZIF-67.

1.3 Synthesis of ZIF-67@PDA:

After the obtained ZIF-67 was uniformly dispersed in a mixed solution of deionized (DI) water and ethanol (1:1, v/v). 5 M Tris was added and stirred for 10 minutes. Subsequently, DAH was added to the ZIF-67 dispersion at a mass ratio of 1:2. The resulting black solution was continuously stirred for 12 hours, then centrifuged to collect the dark gray sample. The sample was washed three times with ethanol and deionized water, followed by drying at 60 °C for 12 hours to obtain ZIF-67@PDA.

1.4 Synthesis of the hollow CoNi-LDH@PDA:

Under ultrasonic conditions, 0.4 g of ZIF-67@PDA were uniformly dispersed in 200 mL of ethanol, designated as solution A. Separately, 0.4 g of $\text{Ni}(\text{NO}_3)_2 \cdot 6\text{H}_2\text{O}$ were dissolved in 50 mL of ethanol, designated as solution B. Solution B was then added to solution A, and the mixture was stirred for 1 hour. The resulting mixture was filtered, washed three times with ethanol, and then dried at 60 °C for 12 hours to obtain CoNi-LDH@PDA.

1.5 Synthesis of CoNiFe-LDH@PDA and CoFe-LDH@PDA:

0.2 g of CoNi-LDH@PDA were added to 50 mL of ethanol and uniformly dispersed using ultrasound. Subsequently, 0.4 g of FeCl₂·4H₂O were added and the mixture was stirred for 3 hours. The resulting mixture was then filtered, washed three times with ethanol, and dried at 60 °C for 12 hours to obtain CoNiFe-LDH@PDA. The preparation method for CoFe-LDH@PDA is essentially the same as that for CoNiFe-LDH@PDA, with the only difference being that the precursor used is ZIF-67@PDA.

1.6 Synthesis of CoNiFe-Se@NC, CoSe₂@NC, CoNi-Se@NC and CoFe-Se@NC:

The obtained CoNiFe-LDH@PDA and selenium powder were mixed at a mass ratio of 1:1 in an alumina boat and annealed at 500 °C for 6 hours under an Ar/H₂ atmosphere (heating rate of 2 °C min⁻¹) to obtain CoNiFe-Se@NC. The preparation methods for CoSe₂@NC, CoNi-Se@NC and CoFe-Se@NC are similar, with the difference being that the precursors are ZIF-67@PDA, CoNi-LDH@PDA and CoFe-LDH@PDA, respectively.

1.7 Materials characterization:

X-ray diffraction (XRD) analysis was conducted using a Bruker D8 Advance instrument (Germany) with Cu-K α radiation ($\lambda=1.5406\text{\AA}$). The morphology of the samples was examined using Field-emission scanning electron microscopy (FESEM, Hitachi S-4800, Japan) and transmission electron microscopy (TEM, FEI, Tecnai G2 F30). Nitrogen adsorption-desorption isotherms were measured at 77 K using an Autosorb-iQ automatic volumetric instrument. The elemental ratio of Fe : Co : Ni : Se was determined by inductively coupled plasma-atomic emission spectrometry (ICP-OES, Thermo Fisher, iCAP 7200 Duo) after acid digestion.

1.8 X-ray absorption spectroscopy:

The X-ray Absorption Fine Structure spectra were obtained for the Fe K-edge (7112 eV), Co K-edge (7709 eV), and Ni K-edge (8333 eV) using the transmission mode at the BL14W1 beamline of the Shanghai Synchrotron Radiation Facility (SSRF) in China. The facility's storage rings operated at an energy of 3.5 GeV with an electron beam current of 230 mA. At the BL14W1 beamline, the X-ray beam was monochromatized with a double-crystal monochromator (DCM) utilizing Si (111) crystals. A Lytle

detector was employed to capture the fluorescence signal, and the energy was calibrated using metal foils. During the fitting process, the theoretical curved-wave backscattering amplitude ($F_j(k)$), phase-shift functions ($\phi_j(k)$), and the mean free path (l) in angstroms (\AA) for all scattering paths were computed using the FEFF8.2 code developed by the University of Washington. By integrating these calculated values into the fitting models, researchers can analyze and interpret the experimental XAFS spectra concerning the local atomic structure and electronic properties of the sample.

1.9 Theoretical calculation:

All spin-polarized calculations were conducted using density functional theory (DFT) as implemented in the Vienna Ab initio Simulation Package (VASP). Valence electrons were accounted for using a plane wave basis set with a kinetic energy cutoff of 500 eV. The generalized gradient approximation (GGA) with Perdew–Burke–Ernzerhof (PBE) functionals was employed to evaluate the electron exchange–correlation energy, with an electron convergence criterion of 10^{-5} eV and an ionic convergence criterion of 0.02 eV \AA^{-1} .

For adsorption and migration calculations, a vacuum space of 15 \AA was established to mitigate interactions between adjacent slabs. A $2 \times 2 \times 1$ k-point mesh was utilized for the systems Fe_2CoSe_4 , CoNiSe_2 , Fe_2NiSe_4 and $\text{Co}_{1.68}\text{Ni}_{0.68}\text{Fe}_{1.38}\text{Se}_4$. The electron density difference was calculated by subtracting the charge densities of Na atoms and each configuration from their corresponding compounds. This charge density difference provides insight into the bonding processes or charge transfer that occurs before and after structural relaxation. The charge density difference of the system can be determined using the following equation:

$$\Delta\rho = \rho_{AB} - \rho_A - \rho_B$$

where ρ_{AB} represents the composition, ρ_A base, and ρ_B absorbate. In the calculation of the latter two quantities, the atomic positions were fixed to those they occupied in the AB system. Van der Waals interactions were considered using the empirical correction of Grimme's scheme (DFT-D3). Additionally, the climbing image-nudged elastic band (CINEB) method was employed for sodium ion migration calculations.

1.10 Electrochemical Measurements:

A slurry was prepared by mixing CoNiFe-Se@NC, Super P and sodium alginate in a mass ratio of 8:1:1 using deionized water as solvent and coated onto copper foil. The coated foil was then dried in a vacuum oven at 60 °C for 12 hours. Electrodes with a diameter of 13 mm were cut from the coated foil, with a loading of approximately 1.0 ~ 1.2 mg cm⁻². CR2032-type button cells were assembled in a glove box (Vigor-LG 2400/750TS, LTD, Suzhou) with oxygen and water contents < 0.1 ppm. Sodium metal (15.6 × 0.45 mm) served as the counter and reference electrode, separated by Whatman GF/D, and 1.0 M NaCF₃SO₃ in diethylene glycol dimethyl ether (DIGLYME) was used as the electrolyte. Constant current and rate performance charge-discharge tests were conducted using a multi-channel battery testing system (CT2001A, LAND). CV and EIS measurements were conducted using a CHI 660 electrochemical workstation (Shanghai Chi-Chi Instrumentation Co., Ltd.) at room temperature. CV scanning voltage ranged from 0.01 to 3.0 V with a scanning rate of 0.2 ~ 1.0 mV s⁻¹, while EIS frequency ranged from 0.01 to 100000 Hz. For full-cells test, CoNiFe-Se@NC and Na₃V₂(PO₄)₃@C were used as anode and cathode electrode, correspondingly. The Na₃V₂(PO₄)₃@C electrodes were prepared by dispersing Na₃V₂(PO₄)₃@C, Super P and polyvinylidene fluoride (PVDF) in N-methylpyrrolidone (NMP) according to a mass ratio of 8:1:1 to form a slurry, and coated on an aluminum foil. The coated foil was then dried in a vacuum oven at 60 °C for 12 hours. Na₃V₂(PO₄)₃@C electrode sheet is the same size as CoNiFe-Se@NC electrode sheet. The loading of each cathode sheet is approximately 2.4 mg cm⁻². The Na₃V₂(PO₄)₃@C half-cell assembly is the same as the CoNiFe-Se@NC half-cells, with the only difference being that the voltage range of the Na₃V₂(PO₄)₃@C test is 2.2 V – 3.8 V. The CoNiFe-Se@NC anode and Na₃V₂(PO₄)₃@C cathode were assembled into a full cell according to the mass ratio of 1:4, in addition to the voltage range was increased to 0.5 V – 3.5 V.

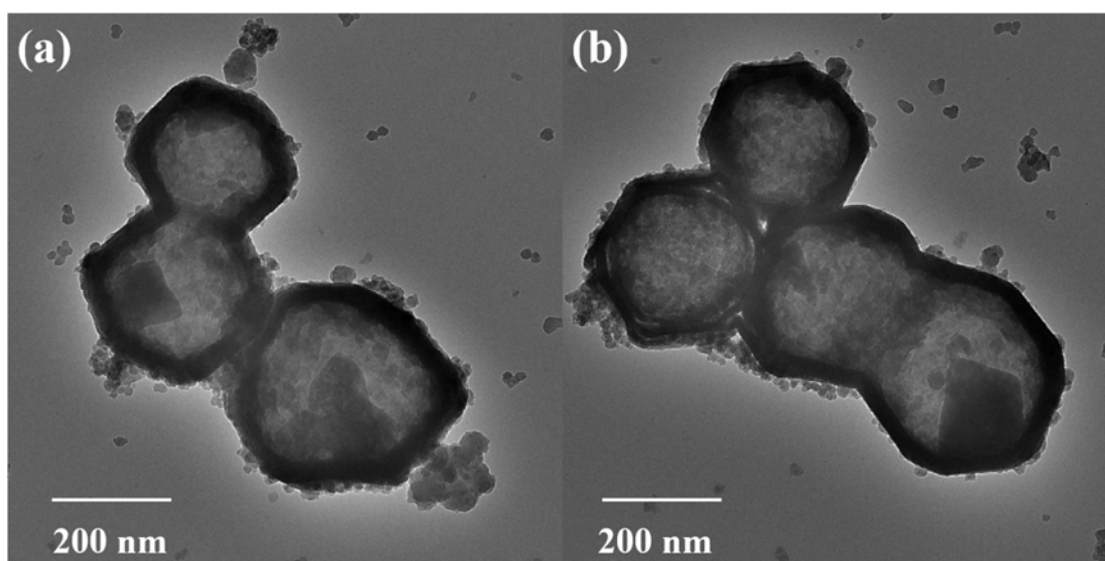


Figure S1. TEM images of CoNi-LDH@PDA and CoFe-LDH@PDA.

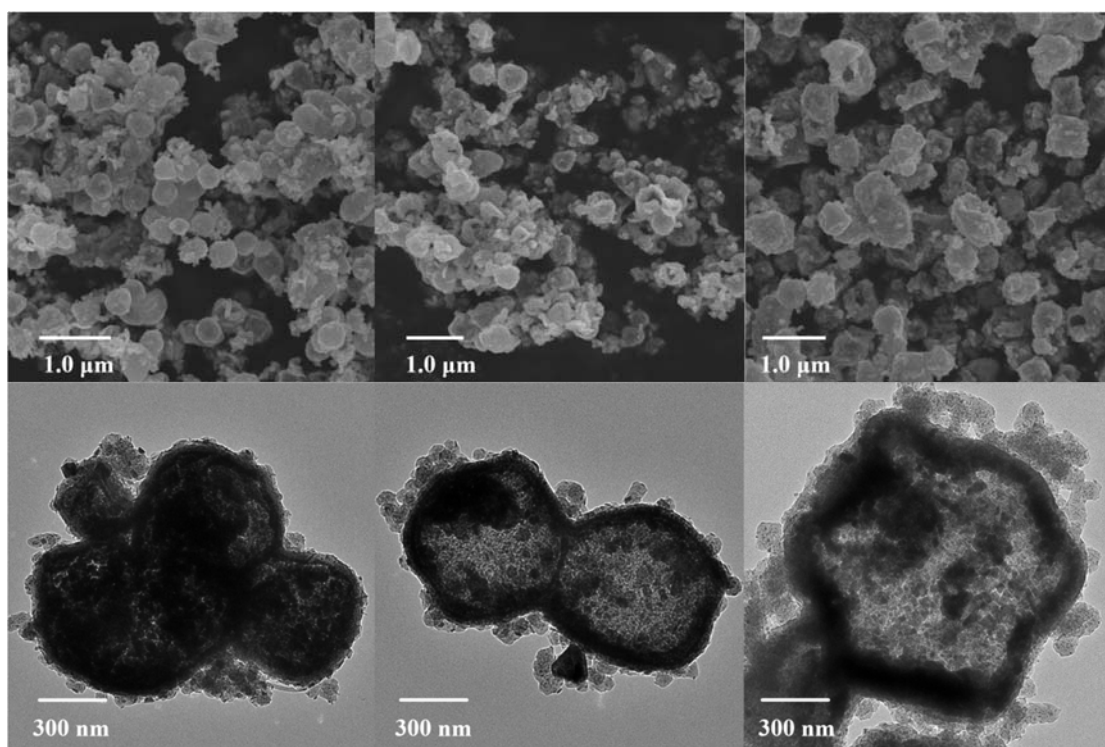


Figure S2. (a) SEM and (d) TEM images of CoSe₂@NC. (b) SEM and (e) TEM images of CoNi-Se@NC. (c) SEM and (f) TEM images of CoFe-Se@NC.

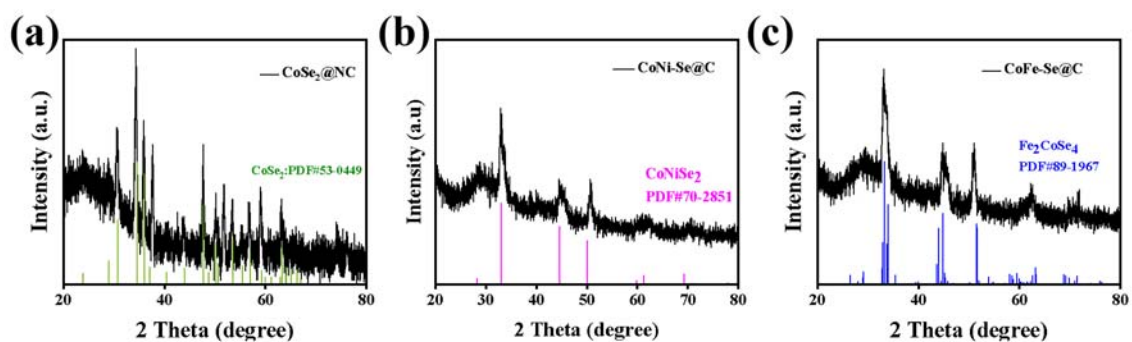


Figure S3. XRD patterns of (a) CoSe₂@NC, (b) CoNi-Se@NC and (c) CoFe-Se@C.

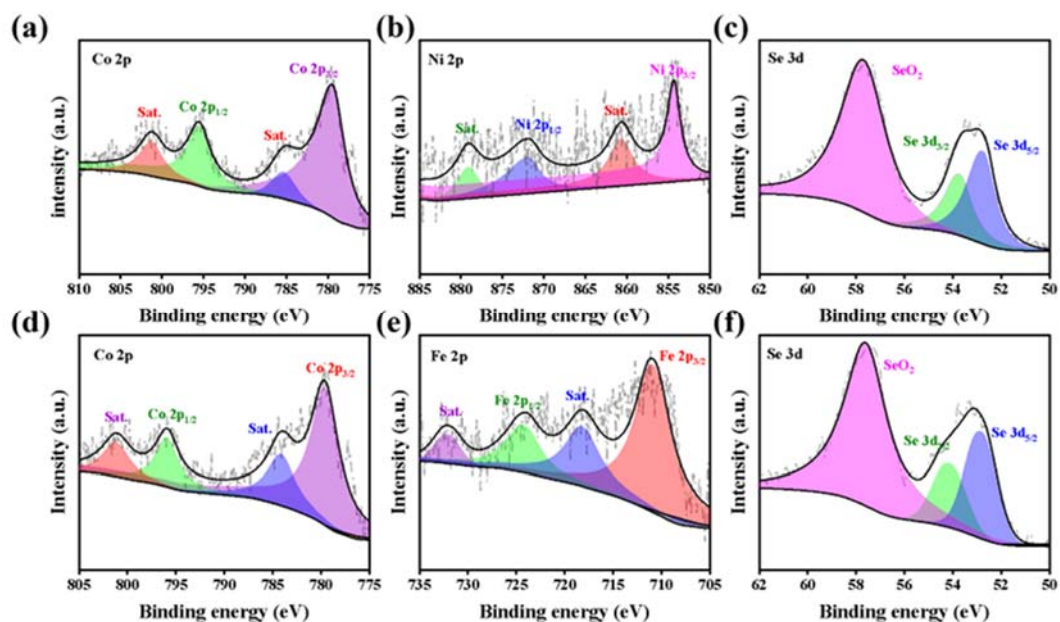


Figure S4. High-resolution XPS spectra of (a) Co 2p, (b) Ni 2p and (c) Se 3d of CoNi-Se@NC. High-resolution XPS spectra of (d) Co 2p, (e) Fe 2p and (f) Se 3d of CoNi-Se@NC.

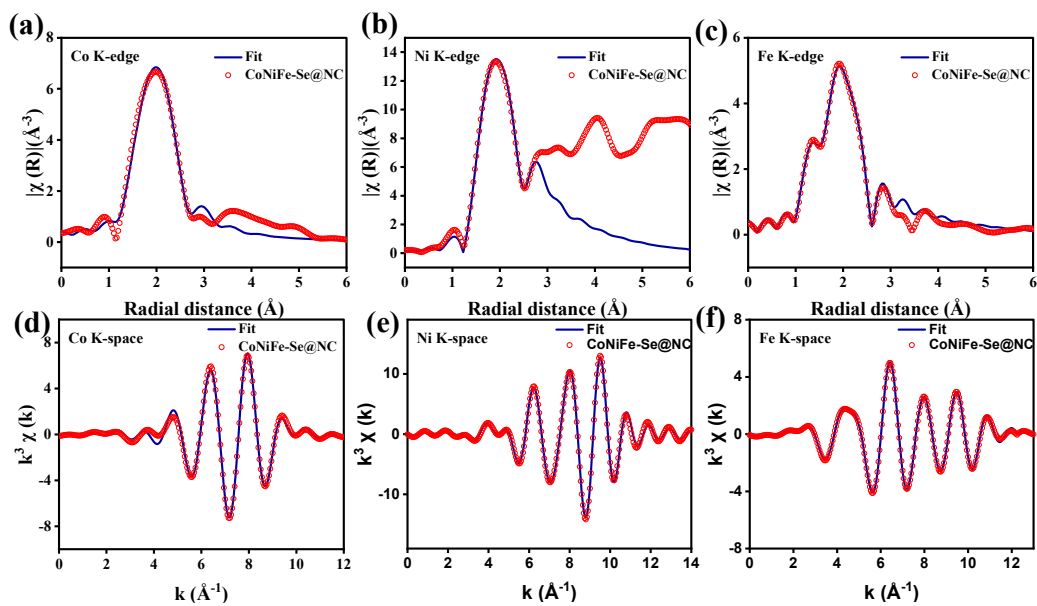


Figure S5. The EXAFS fitting curve of (a) Co, (b) Ni and (c) Fe for CoNiFe-Se@NC in R space and (d) Co, (e) Ni and (f) Fe in k space.

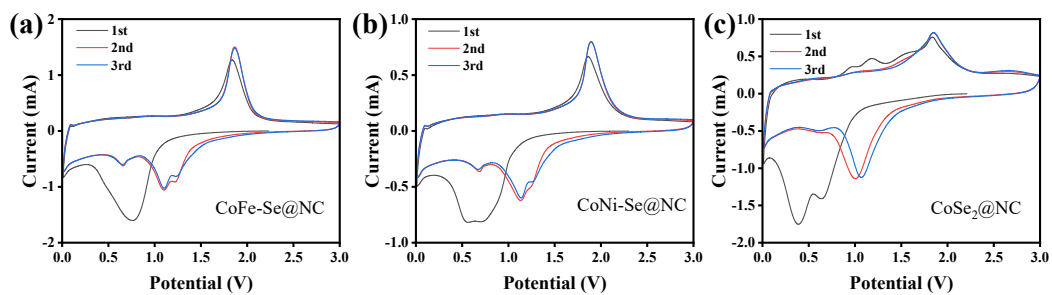


Figure S6. CV curves at 0.8 V s^{-1} of (a) CoFe-Se@NC, (b) CoNi-Se@NC and (c) CoSe₂@NC anode of sodium ion batteries.

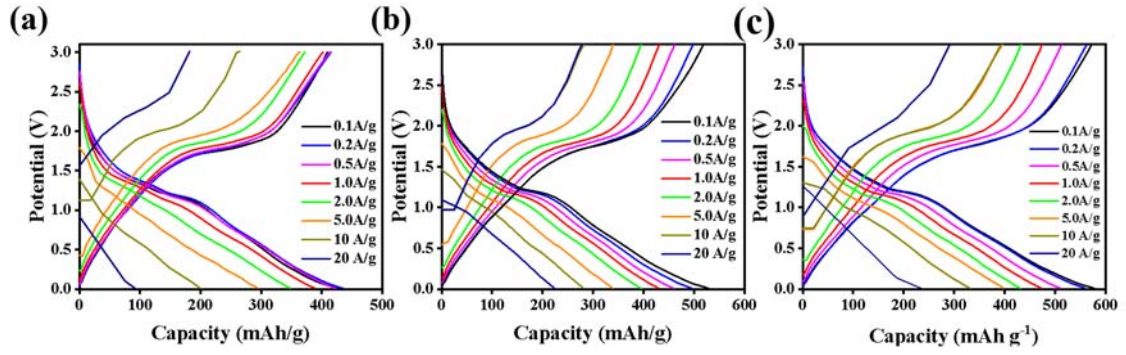


Figure S7. Discharge/charge curves at various rates of (a) CoSe₂@NC, (b) CoNi-Se@NC and (c) CoFe-Se@NC.

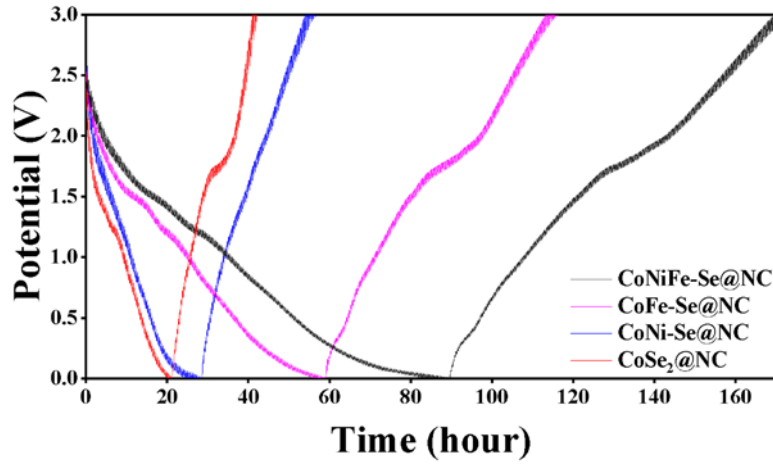


Figure S8. GITT curves of CoSe₂@NC, CoNi-Se@NC, CoFe-Se@NC and CoNiFe-Se@NC.

Based on the results from GITT testing, the diffusion coefficient of Na⁺ can be calculated using Fick's second law with the following equation:

$$D_{Na^+} = \frac{4}{\pi\tau} \left(\frac{m_B V_m}{M_B S} \right)^2 \left(\frac{\delta E_s}{\delta E_t} \right)^2 \quad (1)$$

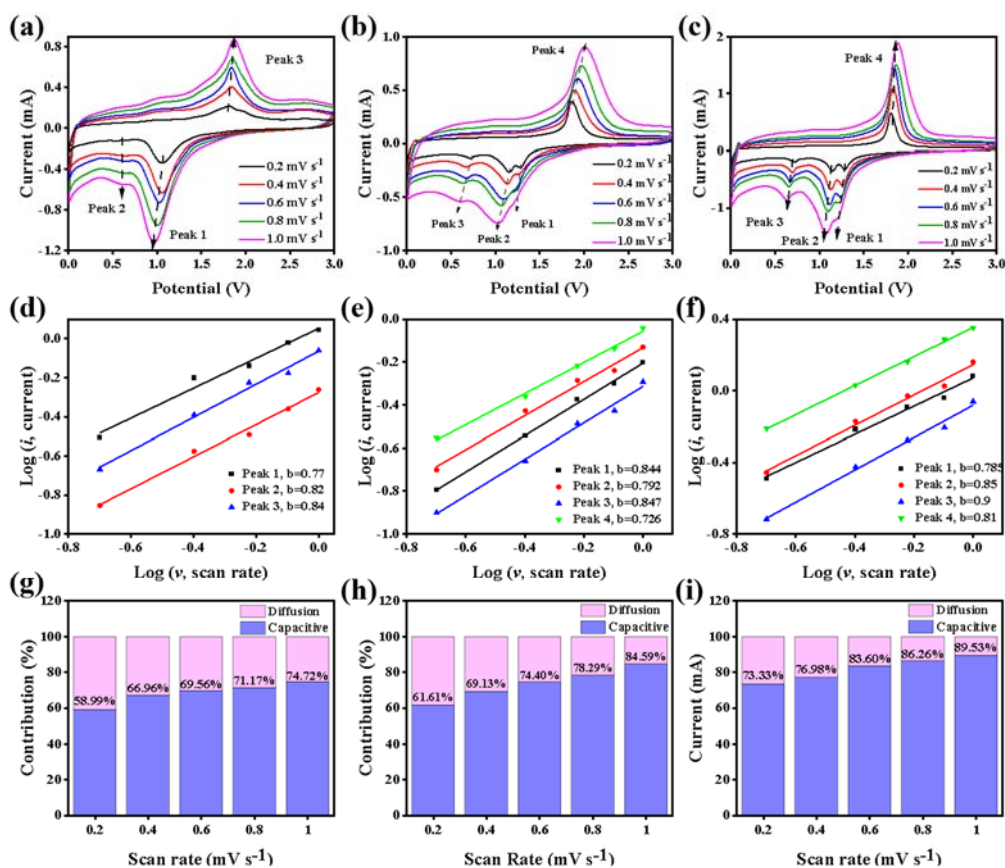


Figure S9. Electrochemical kinetic analysis. For **CoSe₂@NC**: (a) CV curves at various scan rates. (d) The corresponding $\log(i)$ versus $\log(v)$ plots at each redox peak. (g) Contribution rates of capacitive-controlled and diffusion-controlled capacities at different scan rates. For **CoNi-Se@NC**: (b) CV curves at various scan rates. (e) The corresponding $\log(i)$ versus $\log(v)$ plots at each redox peak. (h) Contribution rates of capacitive-controlled and diffusion-controlled capacities at different scan rates. For **CoFe-Se@NC**: (c) CV curves at various scan rates. (f) The corresponding $\log(i)$ versus $\log(v)$ plots at each redox peak. (i) Contribution rates of capacitive-controlled and diffusion-controlled capacities at different scan rates.

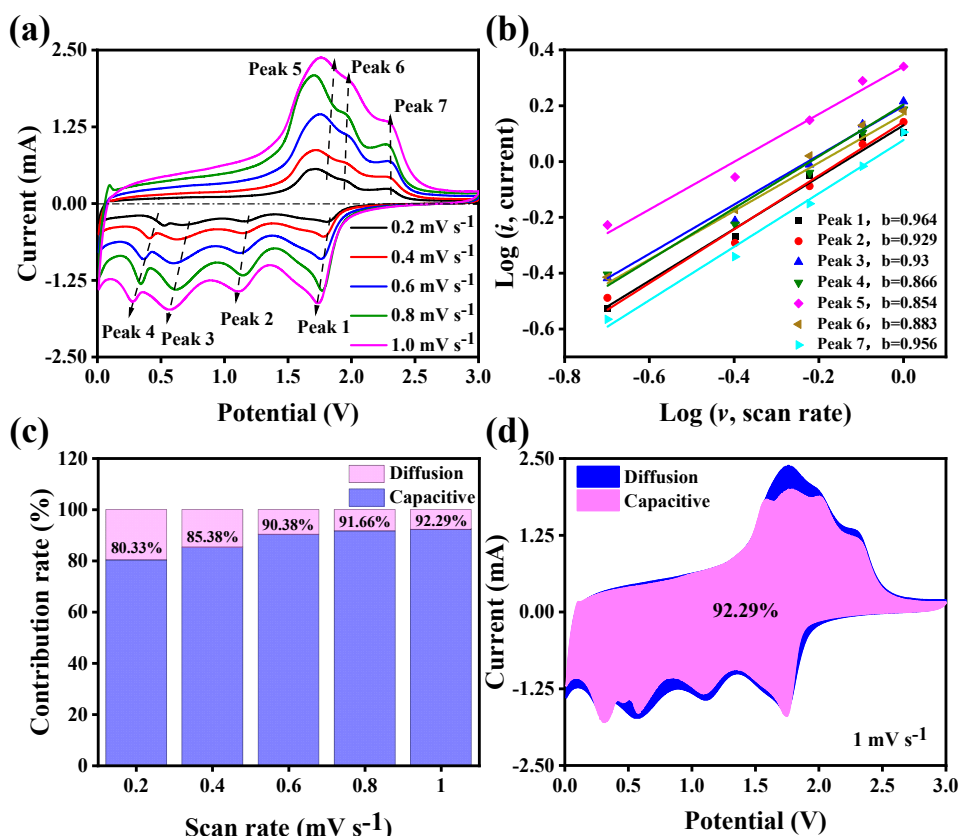


Figure S10. Electrochemical kinetic analysis of CoNiFe-Se@NC electrode in sodium ion batteries. (a) CV curves at various scan rates. (b) The corresponding $\log(i)$ versus $\log(v)$ plots at each redox peak. (c) Contribution rates of capacitive-controlled and diffusion-controlled capacities at different scan rates. (d) Capacitive contribution at 1.0 mV s^{-1} .

Figures S10-11 (Supporting Information) show similar oxidation-reduction peaks in CV curves at different scan rates, indicating good cycle stability. Based on the results from the aforementioned CV curves, equations (2) and (3) were employed to determine the contributions of pseudocapacitance and diffusion¹. Here, i and v in the equations represent the current at each peak in the CV curve and the corresponding scan rate, separately. Furthermore, in equations (2) and (3), a and b are empirical parameters. When b approaches 0.5, the charge/discharge process is primarily diffusion-controlled, whereas when b approaches 1, it is dominated by pseudocapacitance^{2,3}.

$$i = av^b \quad (2)$$

$$\log(i) = b \times \log(v) + \log(a) \quad (3)$$

Further, the contribution of pseudocapacitance can be calculated using equation (4), where k_{1v} and $k_{2v}^{1/2}$ represent the contributions of pseudocapacitance and diffusion control, respectively. As shown in figure 5c, with the scan rate increasing from 0.2 to 1.0 mV s^{-1} , the contribution of pseudocapacitance increases from 80.33 % to 92.29 %. This continuous increase in pseudocapacitive contribution with increasing scan rate indicates contribution of surface reaction in charge storage capacity. Additionally, figure 5d visually demonstrates that at a scan rate of 1.0 mV s^{-1} , pseudocapacitance contributes predominantly (highlighted in pink).

$$i(V) = k_{1v} + k_{2v}^{1/2} \quad (4)$$

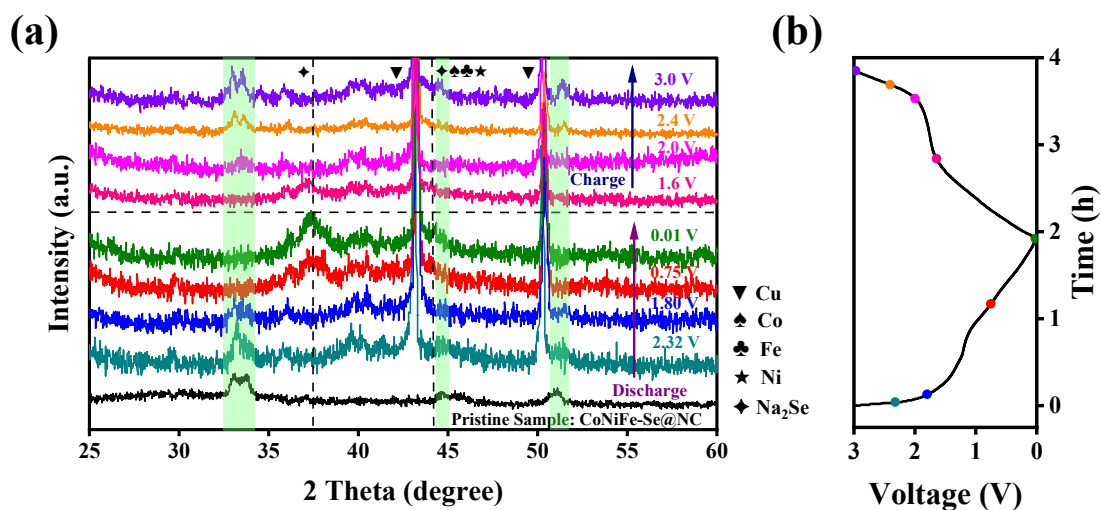
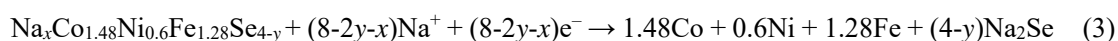
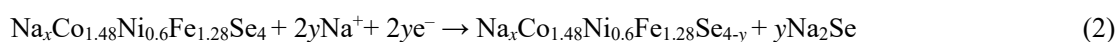
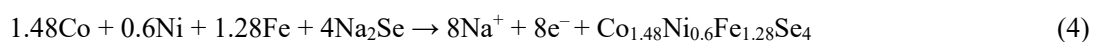


Figure S11. (a) Ex-situ XRD patterns of CoNiFe-Se@NC electrodes during the first charge/discharge cycle. (b) The corresponding charge/discharge curve.

In the cathodic scan, the ingress of Na^+ can be delineated into three stages. Initially, in the first stage, insertion of Na^+ into CoNiFe-Se@NC forms intermediate products $\text{Na}_x\text{Co}_{1.48}\text{Ni}_{0.6}\text{Fe}_{1.28}\text{Se}_4$. In the second stage, further insertion of Na^+ results in $\text{Na}_x\text{Co}_{1.48}\text{Ni}_{0.6}\text{Fe}_{1.28}\text{Se}_{4-y}$ and Na_2Se . In the third stage, $\text{Na}_x\text{Co}_{1.48}\text{Ni}_{0.6}\text{Fe}_{1.28}\text{Se}_{4-y}$ react with Na^+ ions, ultimately transforming into Fe, Co and Ni nanoparticles and Na_2Se . The detailed transformation steps are outlined as follows:



In the anodic scan, metallic Co, Ni and Fe nanoparticles react with Na_2Se , reverting to the original CoNiFe-Se@NC material. The reaction can be described by the following equation:



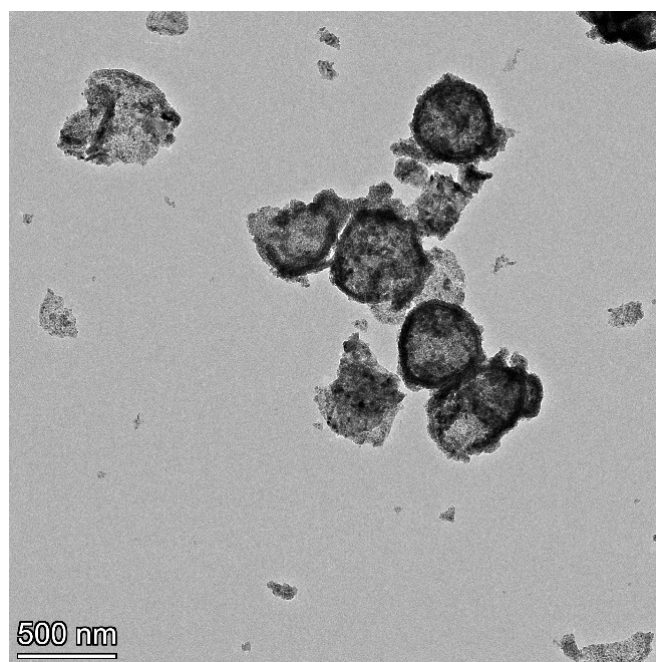


Figure S12. TEM image of CoNiFe-Se@NC after cycling.

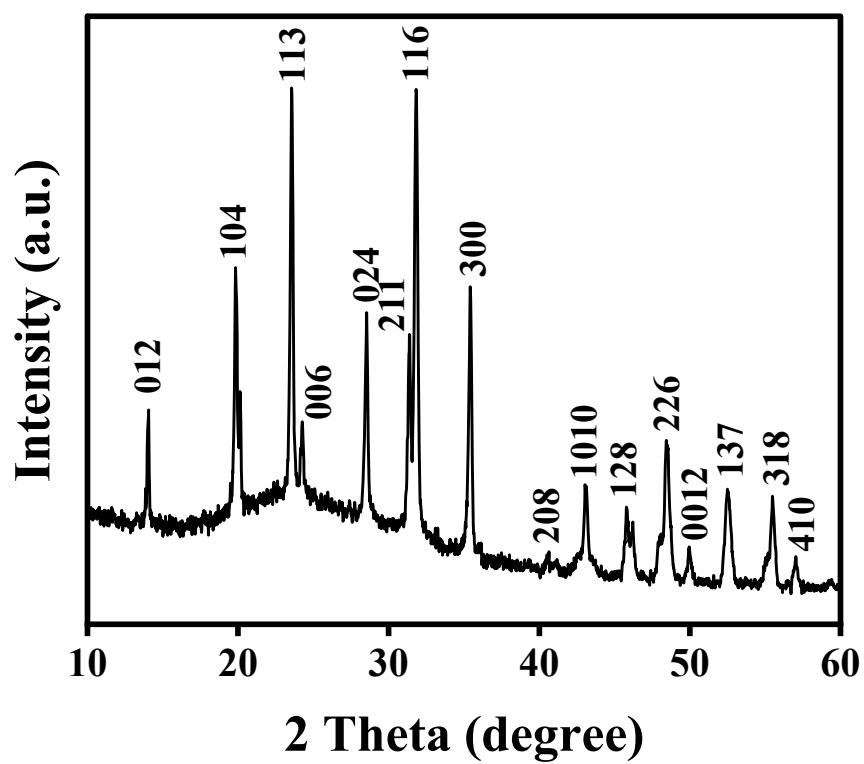


Figure S13. XRD pattern of the Na₃V₂(PO₄)₃@C.

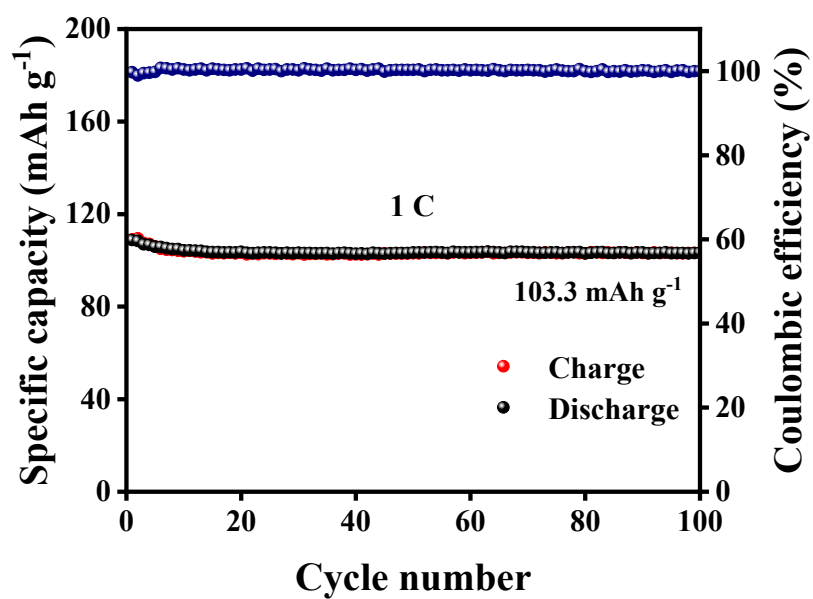


Figure S14. Cycling performance of the $\text{Na}_3\text{V}_2(\text{PO}_4)_3@\text{C}$.

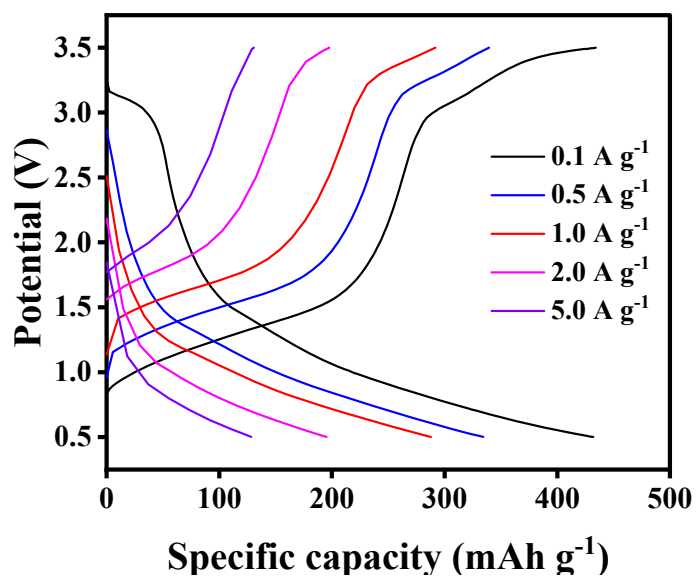


Figure S15. Discharge/charge curves at various rates of NVP//CoNiFe-Se@NC full-cells.

Table S1. Calculation of configurational entropy of CoNiFe-Se@NC, CoFe-Se@NC, CoNi-Se@NC and CoSe₂@NC.

Sample	ΔS_{mix}
CoSe ₂ @NC	$-R(0.3452\ln(0.3452) + 0.6548\ln(0.6548)) \approx 0.644R$
CoNi-Se@NC	$-R(0.2891\ln(0.2891) + 0.1168\ln(0.1168) + 0.5941\ln(0.5941))$ $\approx 0.9189R$
CoFe-Se@NC	$-R(0.2276\ln(0.2276) + 0.1854\ln(0.1854) + 0.587\ln(0.587))$ $\approx 0.962R$
CoNiFe-Se@NC	$-R(0.2236\ln(0.2236) + 0.093\ln(0.093) + 0.1871\ln(0.1871)$ $+ 0.4963\ln(0.4963)) \approx 1.22R$

The formula for calculating mixing entropy is as follows:

$$\Delta S_{\text{mix}} = -R \sum_{i=1}^n x_i \ln x_i$$

where ΔS_{mix} is the entropy, R is the gas constant, and x_i is the molar fraction of the components.

Table S2. The mass loadings of Co, Ni, Fe and Se in CoNiFe-Se@NC measured by ICP-OES and the corresponding atomic percentages.

Elements	Co	Ni	Fe	Se
Mass loading (wt. %)	19.89	8.25	15.72	59.14
Atomic percentage (at. %)	22.36	9.30	18.71	49.63

The formula of CoNiFe-Se in CoNiFe-Se@NC is determined by ICP-AES is $\text{Co}_{1.62}\text{Ni}_{0.68}\text{Fe}_{1.38}\text{Se}_4$.

Table S3. The atomic percentages of Co, Ni, Fe, Se, N and C in CoSe₂@NC, CoNi-Se@NC, CoFe-Se@NC and CoNiFe-Se@NC measured by XPS.

Sample	Co	Ni	Fe	Se	N	C
CoSe ₂ @NC	2.06			3.9	10.72	83.32
CoNi-Se@NC	2.45	0.99		5.04	12.05	79.47
CoFe-Se@NC	2.34		1.91	6.05	13.59	76.11
^a CoNiFe-Se@NC	1.81	0.75	1.57	5.67	11.71	78.49

^a The formula of CoNiFe-Se in CoNiFe-Se@NC is determined by XPS is $\text{Co}_{1.48}\text{Ni}_{0.6}\text{Fe}_{1.28}\text{Se}_4$, quite consistent with that determined by ICP-OES.

Table S4. Fitting parameters for Co, Ni and Fe K-edge EXAFS for CoNiFe-Se@NC.

Sample	Metal element	Bond type	CN	R (Å)	ΔE_0 (eV)	R factor (%)
CoNiFe-Se@NC	Co	Co-Se	2.09	2.34	6.40	0.9
		Co-Se	4.09	2.52		
		Co-M	0.55	2.82		
	Ni	Ni-Se	1.97	2.28	3.12	0.6
		Ni-Se	4.02	2.47		
		Ni-M	0.54	2.73		
		Ni-O	1.02	2.05		
	Fe	Fe-Se	2.05	2.13	5.90	0.1
		Fe-Se	4.03	2.38		
		Fe-M	0.70	2.62		
		Fe-O	1.06	1.95		

M, metal element (Co, Ni, Fe); **CN**, coordination number; **R**, bond distance; ΔE_0 , inner potential correction; **R factor**, goodness of fit.

Table S5. Comparison of the long cycle performance of CoNiFe-Se@NC and metal selenides in half cell from published articles.

Sample	Maximum long-cycle current density (A g ⁻¹)	Cycle number	Specific capacity (mAh g ⁻¹)	References
CoNiFe-Se@NC	10	5000	349.5	Our work
WSe ₂	10	5000	217.4	4
MnSe	1	1000	81.4	5
V-ZnSe/NiSe ₂ @H-NC	2	2000	314.1	6
NiSe ₂ /CoSe ₂	10	1500	296.4	7
Ni-Doped FeSe ₂ /Fe ₃ Se ₄	8	2000	208.8	8
Cu _{2-x} Se@C	5	700	256.3	9
MoSe ₂ NFs	5	1000	328	10
SnSe ₂ /NiSe ₂ @N-Doped	2	5000	335.9	11
CoSe ₂ /C@CNFs	1	2600	247.6	12
Cu ₂ Se@NC	10	2500	246.8	13

Table S6. Comparison of the long cycle performance of NVP//CoNiFe-Se@NC full cells and other metal selenides from published articles.

Sample	current density (A g ⁻¹)	Cycle number	Specific capacity (mAh g ⁻¹)	References
CoNiFe-Se@NC	1	200	264.5	Our work
FeSe ₂	1	100	200	14
Co _{0.85} Se/WSe ₂	0.1	200	224.1	15
CoSe/MoSe ₂ -C	0.5	340	234.6	16
FeSeS	0.5	200	331.9	17
FePSe ₃ @C	0.1	100	78	18
CuSe/ZnSe@NC	0.5	130	153	19
(Co,Cu)Se ₂ /NC	1	200	200.4	20

References

1. Y. Von Lim, S. Huang, Y. Zhang, D. Kong, Y. Wang, L. Guo, J. Zhang, Y. Shi, T. P. Chen, L. K. Ang and H. Y. Yang, *Energy Storage Materials*, 2018, **15**, 98-107.
2. Y. Xia, T. Yang, Z. Wang, T. Mao, Z. Hong, J. Han, D. L. Peng and G. Yue, *Advanced Functional Materials*, 2023, DOI: 10.1002/adfm.202302830.
3. L. Zhao, J. Yin, J. Lin, C. Chen, L. Chen, X. Qiu, H. N. Alshareef and W. Zhang, *ACS Nano*, 2024, **18**, 3763-3774.
4. M. Yu, F. Zeng, Y. Qu, X. Wang, S. Chen, S. Hu, D. Ma, M. Xie and S. Luo, *Energy Storage Materials*, 2024, DOI: 10.1016/j.ensm.2024.103265.
5. S. Chong, T. Li, S. Qiao, Y.-C. Yang, Z. Liu, J. Yang, H.-Y. Tuan, G. Cao and W. Huang, *ACS Nano*, 2024, DOI: 10.1021/acsnano.3c12215.
6. P. Zhou, L. Wang, M. Zhang, Q. Huang, Z. Su, X. Wang, D. Guo, M. Liao, P. Xu and X. Lin, *Chemical Engineering Journal*, 2024, **488**, 150829.
7. H. Fu, Q. Wen, P.-Y. Li, Z.-Y. Wang, Z.-J. He, C. Yan, J. Mao, K. Dai, X.-H. Zhang and J.-C. Zheng, *Small Methods*, 2022, DOI: 10.1002/smtd.202201025.
8. Z. Kong, L. Wang, S. Iqbal, B. Zhang, B. Wang, J. Dou, F. Wang, Y. Qian, M. Zhang and L. Xu, *Small*, 2022, **18**, 2107252.
9. H. Peng, W. Miao, S. Cui, Z. Liu, X. Wang, B. Tao, W. Hou, Z. Zhang and G. Ma, *Chemical Engineering Journal*, 2024, **487**, 150701.
10. H. He, H. Zhang, D. Huang, W. Kuang, X. Li, J. Hao, Z. Guo and C. Zhang, *Advanced Materials*, 2022, **34**, 2200397.
11. H. Li, Y. He, Q. Wang, S. Gu, L. Wang, J. Yu, G. Zhou and L. Xu, *Advanced Energy Materials*, 2023, **13**, 2302901.
12. X. Liu, D. Xue, R. Ren, T. Ou, T. Sun, Y. Han, F. Jin, Y. Li, Y. Zhao and J. Zhang, *Chemical Engineering Journal*, 2024, **496**, 153790.
13. X. Wang, Y. Xu, X. Liu, L. Tan, H. Gu, X. Du and D. Li, *Journal of Energy Chemistry*, 2024, **95**, 336-347.
14. M. Xu, Y. Ma, R. Liu, H. Xiao, L. Chen, Z. Zhang, L. Wang and G. Yuan, *Chemical Engineering Journal*, 2023, **467**, 143382.
15. Y. R. Pei, H. Y. Zhou, M. Zhao, J. C. Li, X. Ge, W. Zhang, C. C. Yang and Q. Jiang, *Carbon Energy*, 2023, DOI: 10.1002/cey2.374.
16. J. Li, Y. He, Y. Dai, H. Zhang, Y. Zhang, S. Gu, X. Wang, T. Gao, G. Zhou and L. Xu, *Advanced Functional Materials*, 2024, DOI: <https://doi.org/10.1002/adfm.202406915>, 2406915.
17. T. Zheng, P. Hu, Z. Wang and T. Guo, *Advanced Materials*, 2023, **35**, 2306577.
18. Z. Tian, W. Sun, J. Yu, J. Yuan, J. Chen, Y. Liu, Y. Ding, X. Hu and Z. Wen, *Advanced Functional Materials*, 2024, DOI: <https://doi.org/10.1002/adfm.202404320>, 2404320.
19. X. Xie, X. Ma, Z. Yin, H. Tong, H. Jiang, Z. Ding and L. Zhou, *Chemical Engineering Journal*, 2022, **446**, 137366.
20. D. Wang, Y. Chao, K. Guo, Z. Wang, M. Yang, J. Zhu, X. Cui and Q. Xu, *Advanced Functional Materials*, 2024, DOI: <https://doi.org/10.1002/adfm.202405642>, 2405642.